# Structural Basis of Substrate Recognition in Human Nicotinamide N-Methyltransferase

Yi Peng,[†] Davide Sartini,[‡] Valentina Pozzi,[‡] Dennis Wilk,[†] Monica Emanuelli,[‡] and Vivien C. Yee*,[†]

[†]Department of Biochemistry, Case Western Reserve University, Cleveland, Ohio 44106, United States
[‡]Dipartimento di Biochimica, Biologia e Genetica, Università Politecnica Marche, Ancona, Italy

ABSTRACT: Nicotinamide N-methyltransferase (NNMT) catalyzes the N-methylation of nicotinamide, pyridines, and other analogues using S-adenosyl-L-methionine as donor. NNMT plays a significant role in the regulation of metabolic pathways and is expressed at markedly high levels in several kinds of cancers, presenting it as a potential molecular target for cancer therapy. We have determined the crystal structure of human NNMT as a ternary complex bound to both the demethylated donor S-adenosyl-L-homocysteine and the acceptor substrate nicotinamide, to 2.7 Å resolution. These studies reveal the structural basis for nicotinamide binding and highlight several residues in the active site which may play roles in nicotinamide recognition and NNMT catalysis. The functional importance of these residues was probed by mutagenesis. Of three residues near the nicotinamide's amide group, substitution of S201 and S213 had no effect on enzyme activity while replacement of D197 dramatically decreased activity. Substitutions of Y20, whose side chain hydroxyl interacts with both the nicotinamide aromatic ring and AdoHcy carboxylate, also compromised activity. Enzyme kinetics analysis revealed k_{cat}/K_m decreases of 2−3 orders of magnitude for the D197A and Y20A mutants, confirming the functional importance of these active site residues. The mutants exhibited substantially increased K_m for both NCA and AdoMet and modestly decreased k_{cat}. MD simulations revealed long-range conformational effects which provide an explanation for the large increase in K_m(AdoMet) for the D197A mutant, which interacts directly only with nicotinamide in the ternary complex crystal structure.
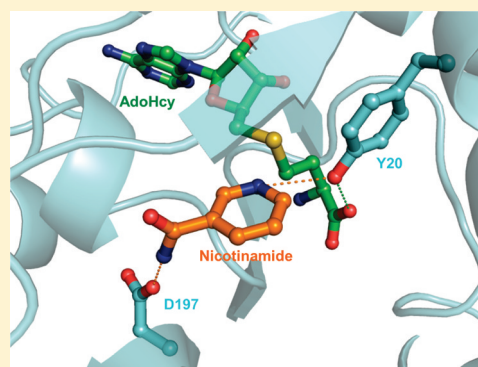
Nicotinamide (NCA) is a compound essential for the formation of NAD(H) and NADP(H), which are involved in many important biological processes, including energy production, cellular resistance to stress, and longevity. Nicotinamide N-methyltransferase (NNMT) is a cytosolic enzyme that catalyzes the N-methylation of NCA, pyridines, and analogues using S-adenosyl-L-methionine (AdoMet) as the methyl donor.[1] NNMT plays a role in NCA metabolism and in the detoxification of many xenobiotics. The enzyme was first characterized in liver[2] where it is mainly expressed; there its activity varies 5-fold among individuals and has a bimodal frequency distribution, which raises the possibility that a genetic polymorphism may be associated with its enzyme activity.[1] In addition, in Parkinson's disease, an enhanced NNMT activity seems to produce toxic N-methylpyridinium compounds, advanced as possible neurotoxins underlying nigrostriatal degeneration.[3,4] Lower expression levels of NNMT are also found in kidney, lung, placenta, heart, brain, and muscle. Interestingly, abnormally high expression of NNMT has been identified in various cancers such as papillary thyroid carcinoma, colorectal cancer, lung cancer, and oral carcinoma.[5−9] To elucidate the structural basis of NNMT catalysis and function and to aid the design of new NNMT inhibitors that may have therapeutic use, crystal structures of NNMT bound to substrate or inhibitor are desirable. Although the crystal structures of human and mouse NNMT (hNNMT and mNNMT, respectively) bound to the demethylated product S-adenosyl-L-homocysteine (AdoHcy) have been determined (unpublished,

PDB accession codes 2IIP and 2I62, respectively), they did not reveal the NCA acceptor substrate binding site. We report here the crystal structure of hNNMT bound to both AdoHcy and NCA. The structure reveals the protein features important for NCA binding and highlights several residues in the active site which were subsequently tested by mutagenesis for their possible importance in NCA recognition and NNMT catalysis.

■ MATERIALS AND METHODS

Cloning, Expression, and Purification. Total RNA was isolated from normal renal tissue using the SV Total RNA Isolation System (Promega). RNA (1 μg) was reverse transcribed with a first strand cDNA synthesis kit II (Bio Basic) using oligo-dT$_{18}$ primers. 0.5 μL of the reaction mixture was then subjected to PCR with Taq polymerase (total volume 25 μL) using the primers 5′-tcacatatggaatcaggcttca-3′ (forward) and 5′-ctaaagctttcacaggggtctg-3′ (reverse) to amplify the human NNMT ORF and to insert NdeI and HindIII restriction sites. The amplified and digested PCR product was cloned into a pT7-7 plasmid vector to obtain the expression construct pT7-7-wt-hNNMT, used to transform E. coli BL21 (DE3) cells that were grown at 37 °C to an OD$_{600}$ of 1.0 before induction with 1 mM IPTG and incubation overnight. Cells were harvested by

centrifugation and resuspended in lysis buffer (10 mM Tris-HCl, pH 8.6, PMSF 1 mM, DTT 1 mM, and aprotinin 2 μg/mL) before sonication and centrifugation. The supernatant was loaded onto a hydroxyapatite column, equilibrated with 10 mM sodium phosphate, pH 7.5, DTT 1 mM, and purified wt-hNNMT eluted with a linear gradient of NaCl from 0 to 1 M in the equilibration buffer.

Extensive crystallization trials failed to yield diffracting crystals of wt-hNNMT. During the course of this work, the crystal structure of a wt-like hNNMT K100A/E101A/E103A triple mutant ("tm") was deposited in the PDB (unpublished, PDB accession code 2IIP). This mutant was designed to facilitate crystallization by reducing the entropy of three surface-exposed residues in a loop distant from the active site. This tm-hNNMT was reproduced using the QuikChange kit (Stratagene) using the primer 5'-ggagaagtggctgaaggcagcgccagcggcctttgactggtcc-3' (substituted nucleotides are underlined) and its complement. Briefly, 25 ng of pT7-7-wt-hNNMT template DNA was incubated with the mutagenic primers, dNTPs, and Pfu DNA polymerase according to manufacturer's recommendations. The full-length tm-hNNMT coding region was then cloned into the NdeI and HindIII sites of a pET-28a plasmid (Novagen) to express N-terminally His6-tagged tm-hNNMT. This pET-28a-tm-hNNMT vector was transformed into E. coli BL21(DE3) cells that were grown at 37 °C to an OD600 of ∼1.0 before induction with 1 mM IPTG and incubation overnight at 25 °C. Cells were harvested by centrifugation and resuspended in lysis buffer (50 mM Tris-HCl, pH 8.0, 0.5 M NaCl, 5 mM imidazole, 2 mM β-mercaptoethanol, and 5% glycerol, 1 mM PMSF) before sonication. After centrifugation, the supernatant was loaded onto Ni-NTA resin (Qiagen) and washed with 50 mM Tris-HCl, pH 8.0, 0.5 M NaCl, 25 mM imidazole, and 5% glycerol. The expressed tm-hNNMT protein was eluted with 50 mM Tris-HCl, pH 8.0, 0.5 M NaCl, 250 mM imidazole, and 5% glycerol. The combined eluted fractions were dialyzed against 50 mM Tris-HCl, pH 8.0, 100 mM NaCl, 5% glycerol, and 1 mM DTT. Final purification was by gel filtration on a Superdex 75 column (Amersham Biosciences) equilibrated with 20 mM Tris-HCl, pH 8.0, 50 mM NaCl, 5% glycerol, and 1 mM DTT.

Crystallization and Data Collection. The purified tm-hNNMT was incubated with AdoHcy at 1:4 molar ratio before concentration to 10 mg/mL, followed by incubation with 10 mM NCA for ∼30 min on ice before crystallization. Crystals of tm-hNNMT bound to AdoHcy and NCA were grown by sitting drop vapor diffusion at 20 °C using a 1:1 protein:precipitant volume ratio from two conditions: 25% PEG3350 in 0.1 M bis-Tris (pH 5.5), and 25−27% PEG3350 with 0.2 M NaCl in 0.1 M Bis-Tris (pH 5.5) or imidazole (pH 6.5). Crystals grew in clusters which needed to be dissected to obtain single crystals for data collection. Cryoprotection in artificial mother liquor containing 35% PEG3350 was followed by flash cooling of the crystals in liquid nitrogen. The best diffracting crystal yielded a 2.7 Å resolution native diffraction data set measured at APS beamline 19ID and processed with HKL[10] (Table 1). The crystal form is not isomorphous to either the tm-hNNMT-AdoHcy or mNNMT-AdoHcy structures deposited in the PDB (accession codes 2IIP and 2I62). The tm-hNNMT ternary complex crystal has space group P1 and contains four molecules in the asymmetric unit/unit cell.

Structure Determination and Refinement. The structure was determined by molecular replacement using the program MOLREP[11] and the protein coordinates from the crystal

Table 1. Data Collection and Refinement Statistics[a]

data collection	
cell dimensions	
a, b, c (Å)	60.7, 61.8, 74.3
α, β, γ (deg)	106.6, 104.0, 104.1
wavelength (Å)	0.97857
resolution (Å)	50−2.7 (2.8−2.7)
R_{sym} (%)	9.1 (47.6)
$I/\sigma I$	9.6 (1.9)
completeness (%)	98.7 (97.5)
redundancy	2.5 (2.4)
refinement	
resolution (Å)	50−2.7 (2.8−2.7)
no. of reflections	23684
R_{work}/R_{free} (%)	20.5/26.4
no. of atoms	
protein, ligand, water	8082, 140, 50
av B-factors (Å^2)	
4 chains: protein, AdoHcy, NCA, water	37.0, 32.1, 48.7, 24.6
protein: chains A, B, C, D	31.1, 31.3, 42.4, 43.4
AdoHcy: chains A, B, C, D	26.7, 21.5, 41.8, 38.2
NCA: chains A, B, C, D	31.4, 38.7, 57.3, 67.3
rmsd[b]	
bond lengths (Å)	0.017
bond angles (deg)	1.678
Ramachandran	
most favored (%)	82.0
additional allowed (%)	18.0
disallowed (%)	0.0

[a]Numbers in parentheses refer to the highest resolution shell. [b]rmsd = root-mean-square deviation.

structure of tm-hNNMT bound to AdoHcy (PDB accession code 2IIP). A 10-residue N-terminal extension, apparently a cloning artifact, was removed from the search model since it is not present in the construct used for crystallization in this work. Iterative rounds of model building were performed with COOT,[12] and refinement calculations were carried out in CNS[13] and REFMAC.[14] A Ramachandran plot calculated with PROCHECK[15] placed 82.0% of the residues in the most favored regions and none in disallowed regions. No density is observed for a couple of residues at the N- and C-termini. The final refined structure includes four molecules of NNMT containing residues 3−261 (chains A−C) or 5−261 (chain D), AdoHcy and NCA ligands bound to each, and 50 water molecules. A summary of the refinement statistics is provided in Table 1. All figures were generated using PyMol.[16]

Preparation of Active Site Mutants. Site-directed mutagenesis to change the selected active site residues was carried out using the QuikChange kit (Stratagene), similarly as described earlier to generate tm-hNNMT from wt-hNNMT. The mutagenic primers used were 5'- atctaagccattttaaccctcgggatgccctagaaaaatattacaagtttg-3' and its complement for the Y20A mutant, 5'- taagccattttaaccctcgggatttcctagaaaaatattacaagttt-3' and its complement for Y20F, 5'- gcagaagttctccgcc ctccccctgggc-3' and its complement for S213A, 5'-gatcatggatgcgctcaaggccagctactacatgattggt-3' and its complement for S201A, and 5'- tcctggtgatcatggctgcgctcaagagcag-3' and its complement for D197A (substituted nucleotides are underlined). The pET-28a-tm-hNNMT plasmid was used as the template for the PCR mutagenesis reaction.

The active site mutants were expressed and purified similarly as for tm-hNNMT, with a few modifications. Induction of transformed bacteria was carried out at 18 °C, and harvested cells were resuspended in a modified lysis buffer (50 mM sodium phosphate, pH 8.0, 0.3 M NaCl, 10 mM imidazole, 0.5 mM DTT, 1 mM PMSF, and 2 μg/mL aprotinin) before sonication. After centrifugation of lysed cells, the supernatant was applied to a Ni-NTA Superflow Cartridge (Qiagen) equilibrated with 50 mM sodium phosphate, pH 8.0, 0.3 M NaCl, 10 mM imidazole, 0.5 mM DTT, and further washed with 50 mM sodium phosphate, pH 8.0, 0.3 M NaCl, 20 mM imidazole, 0.5 mM DTT. The tm-hNNMT mutants were eluted by a linear gradient of imidazole from 20 to 250 mM in 50 mM sodium phosphate, pH 8.0, containing 0.3 M NaCl and 0.5 mM DTT and used to determine catalytic properties.

Enzyme Assays. Initial enzymatic activities were carried out using a 0.45 mL standard assay mixture containing 50 mM Tris-HCl, pH 8.6, 1 mM DTT, 5 mM NCA, 0.5 mM AdoMet and 0.024−0.059 mg/mL of enzyme. Each reaction was started by adding AdoMet, carried out at 37 °C for incubation times ranging between 3 and 60 min, and stopped by adding 100 μL assay mixture to 50 μL of ice-cold 1.2 M HClO$_4$. After 10 min at 0 °C proteins were removed by centrifugation, and 130 μL of the perchloric acid supernatant was then neutralized by adding 35 μL of 0.8 M K$_2$CO$_3$. The resulting KClO$_4$ was removed by centrifugation, and an aliquot of the neutralized supernatant was injected into a Supelcosil LC-18 5 μm reversed phase column (Sigma-Aldrich) and eluted as previously described.[17] The amount of N^1-methylnicotinamide produced was determined by the elution peak areas of the separated compound, with 1 U of enzyme activity representing the formation of 1 nmol of N^1-methylnicotinamide per hour of incubation at 37 °C. For substrate kinetics studies, NCA concentrations were varied from 0.1 to 100 mM, and AdoMet concentrations ranged from 0.01 to 25 mM. Three independent sets of kinetic experiments were carried out and in duplicate each time. Relative enzyme specific activities and enzyme kinetics results are reported in Tables 2 and 3, respectively. Both wt-hNNMT and

tm-hNNMT exhibited similar activity, confirming that alteration of the three surface-exposed residues ∼20 Å from the active site did not compromise enzyme function.

Molecular Dynamics (MD) Simulations. Chain A of the tm-hNNMT-AdoHcy-NCA crystal structure was used as the starting point for modeling and MD simulations. Residues Y20 and D197 were computationally replaced with phenylalanine or alanine to generate initial structural models of Y20F, Y20A, and D197A mutants. AdoHcy, NCA, and crystallographic solvent atoms were removed, and parallel MD simulations of tm-hNNMT and the three mutants were performed using the GROMACS-4.0.7 software package and the G43a1force field.[18,19] The protein structures were first solvated in a cubic periodic box with walls extending 9 Å from the protein coordinates using the SPC water model.[20] Energy was minimized in 400 steps using a steepest descents minimization procedure. In order to solvate the system without distorting the protein models, 30 ps of position-restrained MD was performed before an extended 5 ns MD simulation with coordinates saved for analysis every 1 ps. Polypeptide backbone rmsd values relative to the starting structure were calculated for coordinates saved at different time points during each simulation.

■ RESULTS

Overall Structure of NNMT Ternary Complex. The crystal asymmetric unit contains four conformationally similar copies of hNNMT; pairwise superpositions of the Cα atoms give overall rmsd values ranging from 0.4 to 0.7 Å. Superposition with the previously determined hNNMT-AdoHcy and mNNMT-AdoHcy structures gave similar rmsd values of 0.4 and 1.0 Å, respectively. Electron density for both AdoHcy and NCA was found in all four active sites, but since the average B-factors for NCA and protein are slightly lower for chain A than the other three (Table 1), structural details provided in the following sections are for molecule A unless otherwise noted.

NNMT possesses the class I AdoMet-dependent methyltransferase (MTase) core fold,[21−23] which is comprised of a seven-stranded β sheet flanked by α helices on both sides (Figure 1A). The NNMT structure has several modifications to the MTase core, namely the addition of two α helices at its N-terminus and a reverse β hairpin from Y203-S212 which together form a "cap" over the active site, and two α-helices inserted within W107-A134, adjacent to one set of flanking helices.

A structural similarity search using DALI[24] identified a large number of known and putative MTase structures, of which two stood out as the closest matches: human indolethylamine N-methyltransferase (hINMT) and human phenylethanolamine N-methyltransferase (hPNMT). The hINMT structure is bound to AdoHcy (PDB accession code 2A14, 1.1 Å rmsd

Table 2. Enzyme Activity of hNNMT Proteins[a]

hNNMT	specific activity (×10^3 U/mg of protein)	relative specific activity (%)
wt	9.1 ± 0.5	86
tm-"wt"	10.6 ± 0.5	100
Y20A	0.064 ± 0.007	0.6
Y20F	4.6 ± 0.5	43
D197A	0.250 ± 0.028	2
S201A	8.5 ± 0.4	81
S213A	12.3 ± 0.7	117

[a]Values are given as the means ± standard deviation of three independent sets of experiments, each carried out in duplicate.

Table 3. Enzyme Kinetics of hNNMT Proteins[a]

hNNMT	K_m (mM)		k_{cat} (s^{-1})	k_{cat}/K_m (s^{-1} mM^{-1})	
	NCA	AdoMet		NCA	AdoMet
wt[b]	0.43−0.38	0.0018−0.0022	0.077	0.18−0.2	35−43
tm-"wt"	0.105 ± 0.009	0.0050 ± 0.0006	0.083	0.8	17
Y20A	6.3 ± 0.8	3.5 ± 0.3	0.031	0.005	0.009
Y20F	0.24 ± 0.04	0.028 ± 0.004	0.041	0.17	1.5
D197A	11.8 ± 2.0	2.73 ± 0.16	0.036	0.003	0.013

[a]Values are given as the means ± standard deviation of three independent sets of experiments, each carried out in duplicate. [b]From ref 1.
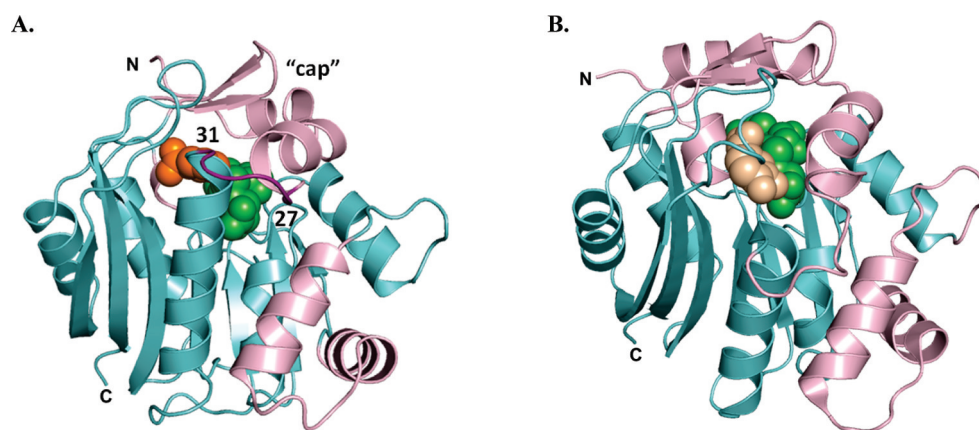
Figure 1. Crystal structure of hNNMT. (A) Ribbon diagram of the hNNMT-AdoHcy-NCA ternary complex. The hNNMT protein (chain A) is colored cyan for the conserved class I AdoMet-dependent MTase core fold and light purple for the nonconserved inserted regions characteristic of the NNMT structure, including the "cap" over the active site and the flexible F27–H31 loop (dark purple). AdoHcy (green) and NCA (orange) are shown as space-filling spheres. (B) Ribbon diagram of the hPNMT-AdoHcy-NA ternary complex crystal structure (PDB accession code 3HCD).[25] AdoHcy (green) and the NA substrate (beige) are rendered as space-filling spheres, and the hPNMT with the conserved core fold in cyan and the PNMT-characteristic inserted regions in light purple.

for 257 superimposed Cα atoms, 52% sequence identity) while of the many hPNMT structures, the most relevant for comparison is that of the ternary complex bound to both AdoHcy and a noradrenaline acceptor substrate (PDB accession code 3HCD, 1.5 Å rmsd for 251 superimposed Cα atoms, 39% sequence identity).[25] The next most similar ternary structure is that of a plant enzyme, 3,7-dimethylxanthine methyltransferase (DXMT), bound to both AdoHcy and a theobromine acceptor substrate (PDB accession code 2EFJ, 3.0 Å rmsd for 200 superimposed Cα atoms, 16% sequence identity).[26] Reflecting their relative degrees of structural and sequence conservation, NNMT, INMT, and PNMT share similar patterns of insertions in the MTase core fold (Figure 1A,B) while DXMT has more extensive additions, particularly in the region capping the active site (not shown).

AdoHcy Binding to NNMT. Electron density corresponding to AdoHcy is very well-defined in all hNNMT molecules (Figure 2A). AdoHcy is bound in a similar position and conformation in NNMT as seen in other class I MTase structures (Figure 1A,B), through extensive hydrogen-bonding and van der Waals interactions. The adenine ring is sandwiched between the hydrophobic side chains of Y86 and A169. In addition, it forms hydrogen bonds to hNNMT, to the V143 main-chain amide via ring atom N1 (chains A, C, and D), and to the D142 side chain via N6 (chain B). The ligand's ribose hydroxyl groups form hydrogen bonds with the D85 (all four chains) and N90 (chain B) side chains. At the other end of AdoHcy, the homocysteine amine group hydrogen bonds to the carbonyl oxygen atoms of G63 and T163, and the two carboxylate oxygen atoms interact with four side chain hydroxyls, those of Y20, Y25, Y69, and T163 (Figure 2A). As also seen in INMT and PNMT, a constellation of conserved aromatic residues lines the active site. In hNNMT, these are Y20, Y25, and Y69 (interacting with AdoHcy carboxylate), Y11 and F15 (near AdoHcy ribose), Y86 (packs against AdoHcy adenine, is phenylalanine in PNMT and INMT), and Y204.

Nicotinamide Binding to NNMT. The electron density for the NCA acceptor substrate is weaker than for AdoHcy (Figure 2B), consistent with significantly hNNMT higher affinity for AdoMet (low μM) than for NCA (high μM) (ref 1 and Table 3). NCA is bound in the same position, with a small

variation in orientation, in the four hNNMT molecules in the asymmetric unit. In chains A–C, the NCA ligands are in nearly the same orientation, while in chain D the NCA is tilted ~40° (Figure 4A). The NCA density is clearest in chains A and B, and the average refined B-factors for NCA in these two chains are lower than those in the other two chains by almost 2-fold (Table 1); thus, the NCA orientation as bound to chain A is selected as the clearest representative of NCA binding to the hNNMT active site.

NNMT catalyzes the transfer of a methyl group from the sulfur of AdoMet to the NCA ring N1 atom. The distance between the NCA N1 and AdoHcy sulfur atom ranges from 3.5 to 4.2 Å. This range is a little longer than the sum of S–C and N–C single bonds and is consistent with the S_N2-like mechanism presumed for AdoMet-dependent MTases.

Y204, part of the constellation of conserved active site aromatic residues, forms a hydrophobic clamp along with L164 to position the NCA ring. The side chains of three hNNMT residues, D197, S201, and S213, are within hydrogen-bonding distance of the NCA amide (Figure 2B). In addition, the Y20 hydroxyl group is close enough to the other end of the substrate to form electrostatic interactions with the NCA ring.

Structure-Based Mutagenesis of NNMT. To probe the functional importance of the four hydrophilic active site residues interacting with NCA, Y20, D197, S201, and S213 were targeted for mutagenesis. D197A, S201A, and S213A mutants were designed to remove the side-chain hydrogen-bonding interactions with the NCA amide. Y20F and Y20A mutants were prepared to test whether the hydroxyl group or aromatic ring of the side chain is important. Enzyme activity assays were carried out, and the relative specific enzyme activities were compared (Table 2). The Y20F mutant had only modestly diminished activity (to 43%) while the Y20A mutant was much more dramatically compromised (0.6% of wild-type activity). The D197A mutant activity was substantially decreased, to 2.4% that of wt. The other two polar side chains near the NCA amide do not appear to play a role in function, since the S201A and S213A exhibited near wt activity.

Enzyme Kinetics. Detailed enzyme kinetics were then carried out for the three active site mutants with significantly
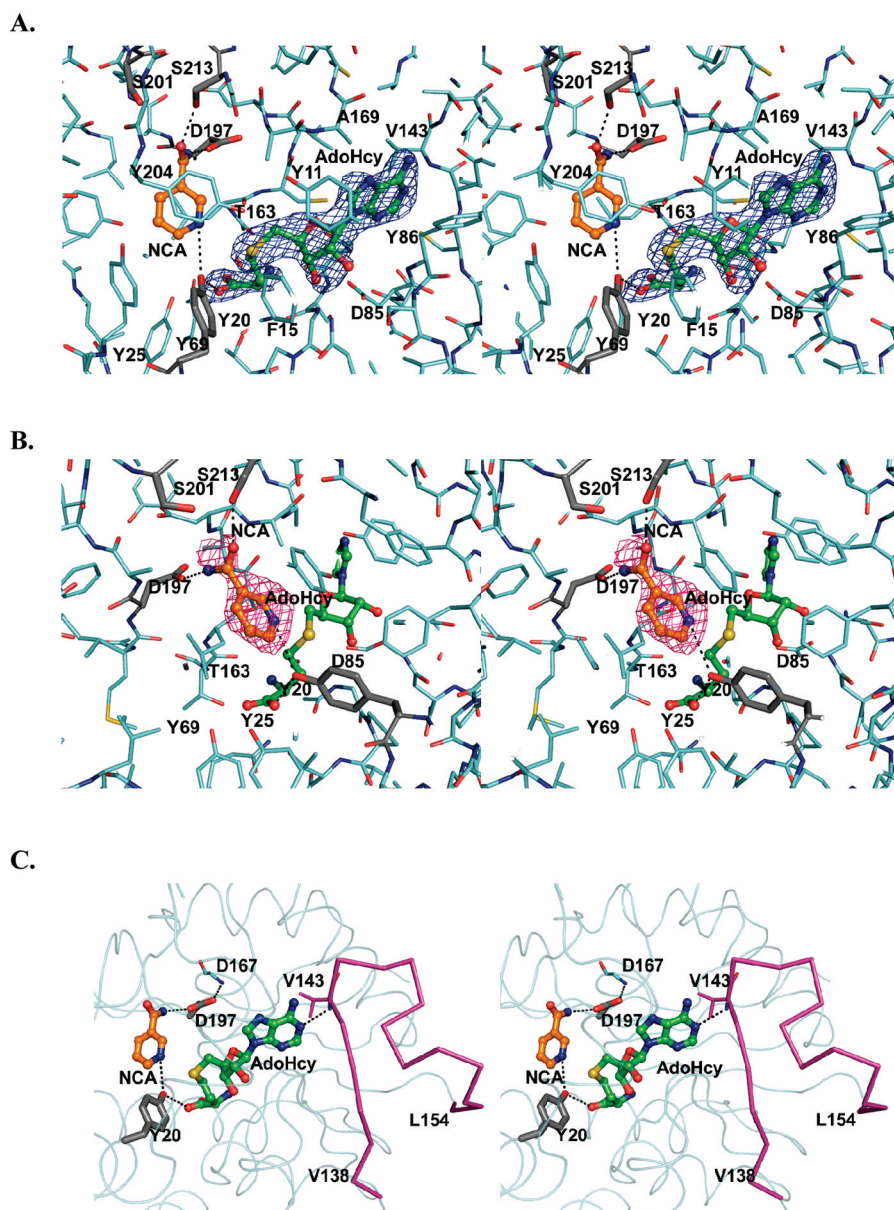
Figure 2. hNNMT-AdoHcy-NCA active site (chain A). (A) Stereoview of the AdoHcy binding site. AdoHcy is shown as a ball-and-stick structure with green carbon atoms; the nearby NCA substrate has orange carbon atoms. Hydrogen bonds involving several residues which interact with NCA (side chains of Y20, D197, S201, and S213 with gray carbon atoms) are represented as dashed lines. The 2.7 Å resolution simulated annealing $|F_o| - |F_c|$ omit density is contoured at 3σ (blue mesh). (B) Stereoview of the NCA binding site. The 2.7 Å resolution simulated annealing $|F_o| - |F_c|$ omit density, contoured at 1.0σ (pink mesh), is weaker than that for AdoHcy but clearly shows the bound NCA. (C) Stereoview of hNNMT region which is conformationally variable in D197A MD simulation. The D197 side chain forms H-bonds to both NCA and the D167 main chain. During MD simulation, the V138-L154 region changes conformation most significantly. Residues in this region interact with the adenine moiety of AdoHcy, explaining how the long-range conformational effects of D197A may influence AdoMet affinity.

decreased activity and compared with wt parameters (Table 3). Values for k_{cat} for the Y20A, Y20F, and D197A mutants were decreased modestly by only ~2-fold compared to wt, while K_m for both NCA and AdoMet were more substantially affected. For Y20A and D197A, K_m(NCA) increased 60- and 112-fold, respectively, while the effect on K_m(AdoMet) was even more dramatic (690- and 546-fold increases, respectively). In contrast, K_m(NCA) and K_m(AdoMet) increased only 2- and 6-fold for Y20F. Because of the differences in K_m consequences, k_{cat}/K_m decreases only modestly for Y20F (5- and 11-fold) and much more significantly for Y20A (159- and 1847-fold) and D197A (258- and 1259-fold).

MD Simulations. Since the Y20 side chain interacts with both NCA and AdoMet (Figure 2A,B), the increases in both K_m(NCA) and K_m(AdoMet) for the Y20A mutant are not surprising. However, D197 interacts only with NCA (Figure 2A); the >500-fold increase in K_m(AdoMet) is not easily predicted by the hNNMT-AdoHcy-NCA crystal structure. MD simulations were carried out to explore the possible structural consequences of the active site mutants. During the course of 5 ns simulations, the D197A conformations deviated more from the initial crystal structure-based model than either wt or the Y20A and Y20F mutants (Figure 3A). When structures at the end of the simulation runs were compared to the starting models, the largest conformational shifts were found to involve
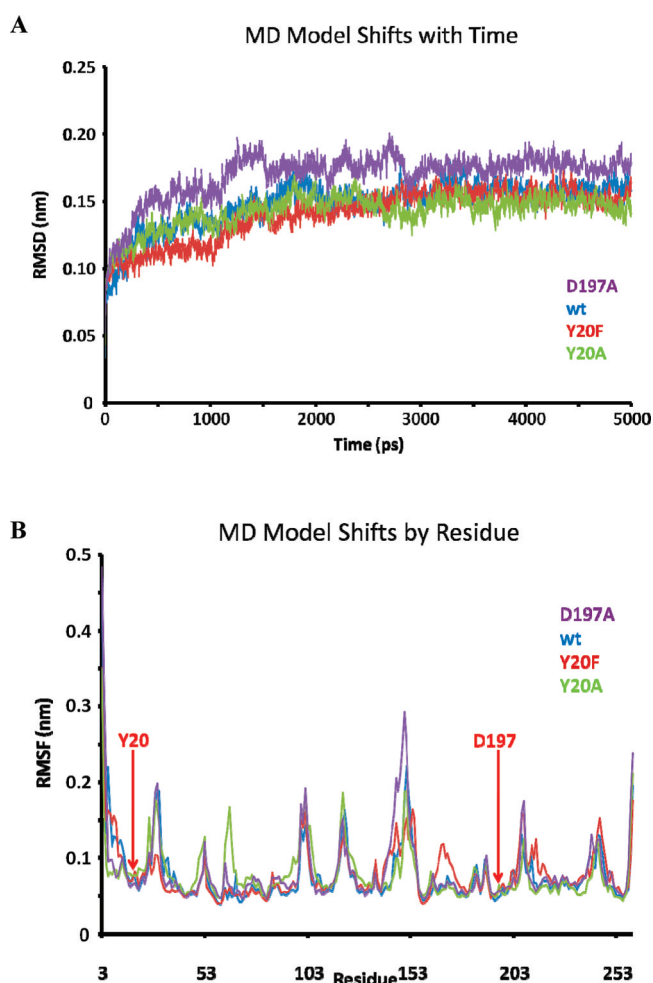
Figure 3. MD simulations of hNNMT. (A) Conformational shifts from starting coordinates for wt and mutant hNNMT structures sampled during the 5 ns simulations, expressed as rmsd for main-chain atoms. The D197A mutant deviates more from the starting structure than the wt or two Y20 mutants. (B) Conformational differences between starting and final coordinates for wt and mutant hNNMT structures for 5 ns simulations, expressed as rmsf (root-mean-square fluctuations) for main-chain atoms for each residue. The largest shifts, for the V138-L154 region, are observed only for the D197A simulations.

residues V138-L154 and in only the D197A simulation (Figure 3B). This segment is distant from the D197A mutation site (Figure 2C), but residues within it interact with the adenine ring of AdoHcy and thus presumably would with AdoMet.

DISCUSSION

Structural comparison of the hNNMT-AdoHcy-NCA ternary complex with the hNNMT-AdoHcy and mNNMT-AdoHcy binary complexes reveals only one major conformational difference: the hNNMT binary complex is missing residues F27-H31 and is presumably disordered in this region. This loop is ordered in both the hNNMT ternary complex and mNNMT binary complex, albeit in different conformations (Figure 4B). Other than this loop, the three NNMT structures are very similar, even though they crystallized in three nonisomorphous crystal forms. AdoHcy is bound in essentially the same position and conformation and interacts with the same protein residues, in all three structures. The NCA binding site is occupied by one

to three water molecules in the binary complex structures (each crystal structure contains four protein molecules in its asymmetric unit). The surrounding protein residues are in the same conformation whether NCA or solvent are bound.

While many structures of AdoMet-dependent methyltransferases have been reported, very few are of enzyme-AdoHcy/AdoMet-acceptor substrate ternary complexes. For comparison with hNNMT-AdoHcy-NCA, the most similar structure is that of hPNMT-AdoHcy-NA (noradrenaline).[25] Structural superposition shows that AdoHcy binds to both hNNMT and hPNMT in the same position and orientation (Figure 4C), which is consistent with the high degree of structural and sequence similarity for the two enzymes. The NCA and NA binding modes are less similar: the two acceptor substrates approach the AdoHcy from the same general direction, but their binding sites only partially overlap (Figure 4C). When the structures are superimposed, NCA bound to hNNMT sterically clashes with hPNMT residue E219, which is a much shorter S201 in hNNMT. Similarly, NA bound to hPNMT sterically clashes with hNNMT residue Y242. This bulky tyrosine residue is at the end of a β-strand in hNNMT that bulges out into solvent in hPNMT due to a two-residue insertion. Thus, while hNNMT and hPNMT have very conserved AdoHcy (and thus presumably AdoMet) binding sites and overall protein folds, their methyl substrate acceptor binding sites have diverged to accommodate very different molecules.

After hPNMT, the next most similar ternary complex is DXMT-AdoHcy-TB (theobromine).[26] Although DXMT and hNNMT are only 16% identical in sequence, they share a similar core protein fold and bind AdoHcy (and thus presumably AdoMet) in similar orientations (Figure 4D). TB is bound to DXMT in two orientations, at a site which only partially overlaps with the NCA binding site in hNNMT (Figure 4D). When the structures are superimposed, NCA bound to hNNMT sterically clashes with DXMT residues Y157 and I226. The homologous residues in hNNMT either have different local protein main chain conformation (L164) or are smaller (A198) so that they do not interfere with NCA binding. TB bound to DXMT sterically clashes with hNNMT residues Y24 and Y204. These are located in nonconserved insertions which are different sizes and conformations in DXMT. Comparison of the hNNMT, hPNMT, and DXMT ternary complexes illustrates the high degree of variation in the acceptor binding sites of AdoMet-dependent methyltransferases that provides for substrate diversity and specificity within a shared protein core scaffold.

The S_N2-like reaction mechanism of AdoMet-dependent methyltransferases involves the direct transfer of a methyl group from AdoMet to the acceptor substrate. The hNNMT-AdoHcy-NCA ternary complex reveals NCA nitrogen to AdoHcy sulfur atom distances ranging from 3.5 to 4.2 Å. These N−S distances are slightly longer than the sum of carbon−sulfur (donor) and carbon−nitrogen (acceptor) single bonds (1.8 and 1.5 Å, respectively) and consistent with what would be expected for an S_N2-like intermediate with a linear arrangement of the N (NCA nucleophile)−C (methyl)−S (AdoHcy leaving group) atoms. The hNNMT AdoHcy−substrate distances are comparable to those seen in the hPNMT and DXMT ternary complexes. In the hPNMT structure, the AdoHcy sulfur to NA nitrogen distance is slightly longer, at 5.5 Å (Figure 4C). In DXMT, TB serves as both substrate and product; DXMT methylates two different TB nitrogen atoms in two separate methylation reactions that combine to produce caffeine. As a result, there are two
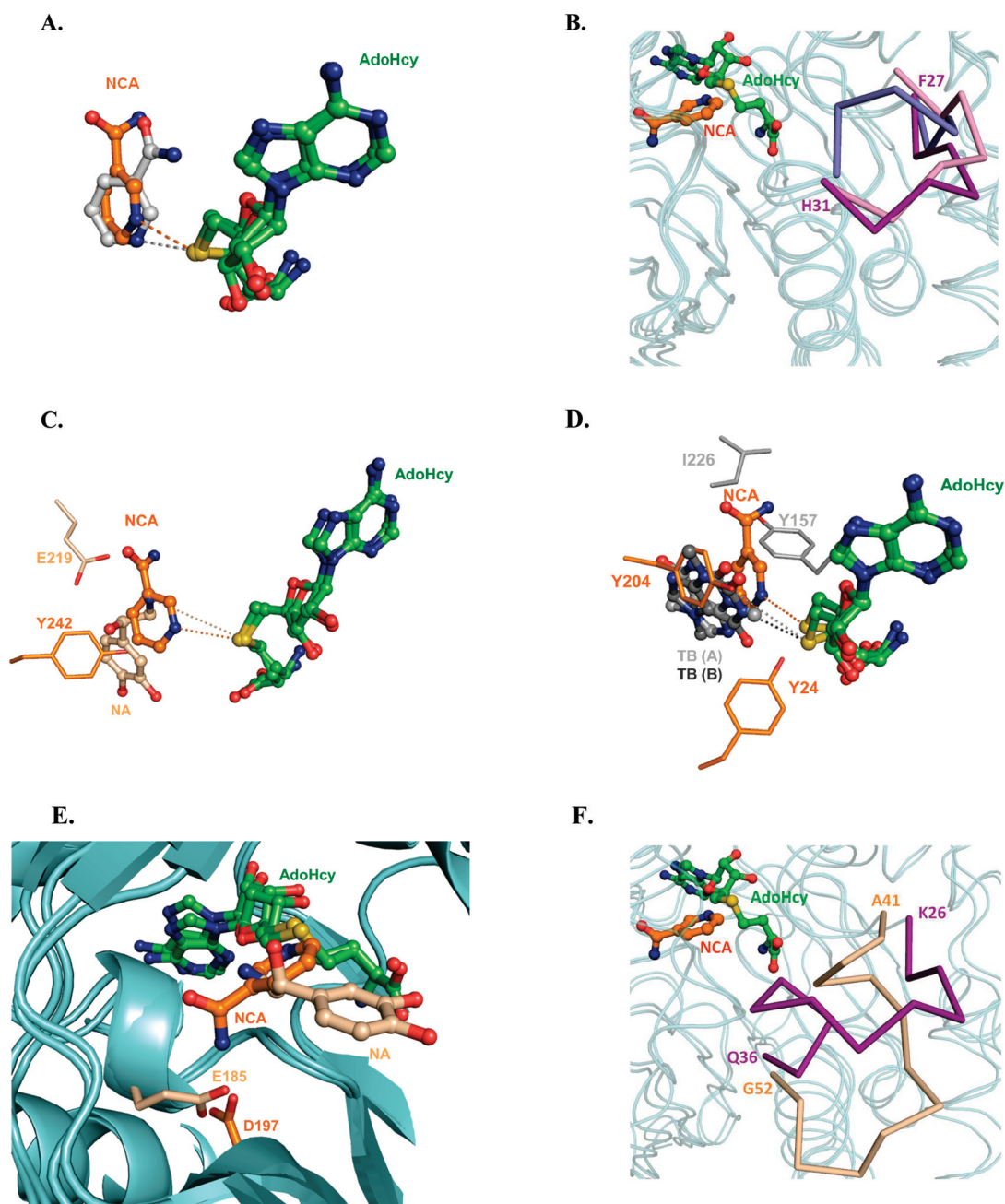
Figure 4. AdoHcy and acceptor substrate binding in hNNMT and other MTases. (A) AdoHcy and NCA bound to hNNMT. The four AdoHcy bound to the four superimposed hNNMT have essentially identical conformations (green carbon atoms). NCA is bound similarly in chains A (orange carbon atoms, shown), B and C (not shown), and in a second slightly different orientation in chain D (light gray carbon atoms). Dashed lines represent the possible path of methyl transfer between the AdoHcy sulfur atom and NCA acceptor nitrogen atom. (B) A surface loop containing residues F27−H31 in the hNNMT-AdoHcy-NCA ternary complex (purple Cα trace) adopts a different conformation than the homologous loops in the mNNMT-AdoHcy (light blue) and hINMT-AdoHcy (light pink) structures. The rest of the protein structures are shown as light cyan backbone coils. (C) Comparison of hNNMT and hPNMT ligands. AdoHcy binds to hNNMT and hPNMT similarly. hNNMT-bound NCA (chain A orientation) and hPNMT-bound NA (beige carbon atoms) approach their respective AdoHcy from the same direction, but bind in very different orientations. Dashed lines show the path between the AdoHcy sulfur atom and acceptor nitrogen atoms in the two substrates. (D) Comparison of hNNMT and DXMT ligands. AdoHcy binds to hNNMT and DXMT similarly. The DXMT TB substrate binds in two orientations in the active site (ball-and-stick with dark and gray carbon atoms, PDB accession code 2EFJ),[26] both of which are different from the orientation of hNNMT-bound NCA. (E) Comparison of NNMT and PNMT active sites. Mutagenesis of D197 in NNMT (side chain with orange bonds involving carbon atoms) and E185 in PNMT (side chain with beige bonds involving carbon atoms) substantially decrease activity in their respective enzymes. (F) The F27−H31 loop conformational divergence when comparing the hNNMT and hPNMT ternary complex structures is greater since an adjacent segment is helical in hNNMT (purple) but unwound in hPNMT (beige).

different TB binding modes in the DXMT crystal structure that position the two different nitrogen atoms to approach the AdoHcy (Figure 4D) with TB nitrogen atom to AdoHcy sulfur

atom distances of 3.6 and 4.5 Å, very similar to those seen in the hNNMT-AdoHcy-NCA complex structure. While NCA is bound to two slightly different orientations in hNNMT, both position

the same nucleophilic ring nitrogen atom to approach AdoHcy. The more common NCA orientation has a shorter NCA nitrogen–AdoHcy sulfur distance (3.5–3.8 Å, chains A–C) while the less common NCA orientation (chain D) has a longer NCA–AdoHcy distance of 4.2 Å (Figure 4A); the difference between these two distances is not very significant given an estimated average coordinate error of 0.4 Å based on the correlation of R_{free} with data resolution for the refined NNMT-AdoHcy-NNMT structure. The two NCA orientations differ by about 40°, but both allow reasonable bond angles about the AdoMet sulfur atom consistent with tetrahedral geometry when a methyl group is modeled in line between the AdoHcy sulfur and NCA nitrogen. Thus, based on AdoHcy–NCA distances and modeled AdoMet sulfur geometry, both NCA orientations are likely to be productive for catalysis.

Inspection of the hNNMT-AdoHcy-NCA structure identified several hydrophilic residues, conserved in NNMT sequences (Figure 2B). The Y20 side-chain hydroxyl group interacts with the AdoHcy carboxylate and the NCA ring; Y20F and Y20A mutants were prepared to investigate the functional importance of the hydroxyl group. The S201 and S213 hydroxyl groups, and the D197 carboxylate, interact with the NCA amide; S201A, S213A, and D197A mutants were investigated to probe the functional role of these side chains. Of the five mutants, enzyme activity was dramatically diminished for only Y20A and D197A (Table 2). Y20F had only modestly compromised activity, suggesting that Y20s importance lies in its aromatic ring, perhaps by packing against and orienting AdoMet, NCA, and surrounding hydrophobic residues, rather than primarily in the electrostatic interactions involving its hydroxyl. Subsequent enzyme kinetics analysis revealed that k_{cat}/K_m was diminished only modestly for Y20F, and much more substantially for Y20A and D197A mutants, due to dramatic increases in K_m for both NCA and AdoMet, and only a modest decrease in k_{cat} (Table 3). These results suggest that both residues are important for binding for both methyl donor and acceptor.

Since the D197 side chain interacts directly with NCA, the effect on K_m(NCA) is expected; the cause for the increased K_m(AdoMet) is less clear. MD simulations revealed that the D197A structures deviate more from the starting crystal-structure-based model than either wt or Y20A/F mutants (Figure 3A). The largest conformational shifts were seen only during the D197A simulation and involved residues V138-L154 (Figure 3B). The hNNMT-AdoHcy-NCA crystal structure shows that residues C141-T144 in this segment pack against AdoHcy, and the V143 main chain nitrogen is within H-bonding distance with the AdoHcy adenine (Figure 2C). These long-range conformational shifts seen only in the D197A MD simulation explain how the D197A substitution leads to a large increase in K_m(AdoMet) despite not directly interacting with the methyl donor. It is interesting to note that when the hNNMT and hPNMT ternary complex structures are superimposed, the carboxylate groups of the hNNMT D197 and hPNMT E185 occupy approximately the same position in space (Figure 4E). In hNNMT, the D197 carboxylate directly interacts with the NCA amide (distances range from 3.0 to 3.9 Å with no nearby solvent molecules in chains A–D) while in hPNMT, the E185 carboxylate is a more distant 5.2 Å with an intervening solvent molecule and is proposed to carry out water-mediated deprotonation of its substrate.[25,27] The pK_a for the hNNMT substrate, NCA, at 3.3 is much lower than the pK_a

of 8.4 for the hPNMT NA substrate, and thus a substrate deprotonation step is unlikely to be important in the NNMT reaction. Since hNNMT D197 and hPNMT E185 are not located in homologous positions in the amino acid sequence of their respective proteins, their spatial convergence is striking considering the different roles they appear to play in acceptor substrate binding and enzyme mechanism.

Comparison of the hNNMT, hPNMT, and DXMT ternary complex structures reveals the details of how these three enzymes share a common core protein fold and yet can accommodate binding of diverse acceptor substrates in different binding modes. Comparison of these, and the hINMT-AdoHcy binary structure, highlights a flexible region which may contribute to allowing diverse substrates to bind to different AdoMet-dependent MTases. In hNNMT, a surface loop containing residues F27–H31 is disordered in the absence of NCA but ordered when the substrate is bound. This loop is ordered in the mNNMT binary complex but adopts a different conformation although all the loop residues are conserved (Figure 4B). It is interesting to note that the corresponding loop in the hINMT binary complex is in a third conformation which is similar to that in the hNNMT ternary complex, despite the low 20% loop sequence conservation. The hNNMT F27–H31 loop is in an insertion region that is not part of the conserved AdoMet-dependent MTase core fold. The corresponding loop region in hPNMT shows even greater conformational divergence: one turn of the adjacent conserved helix is unwound relative to hNNMT, and the longer loop adopts a very different conformation (Figure 4F). This surface loop is one of only three significant differences in protein main-chain conformation between hNNMT and hPNMT ternary complex structures: the other two are the previously mentioned β-bulge that accommodates acceptor substrate binding to hPNMT and the N-terminus which forms part of the cap over the AdoHcy-bound portion of the active site. This surface loop does not directly interact with acceptor substrates in the ternary complexes, but it is located ~10–15 Å away in the various structures and is part of the nonconserved insertions which cover the active site.

In conclusion, the hNNMT-AdoHcy-NCA ternary complex structure identifies active site residues which define the acceptor substrate binding pocket; of these, Y20 and D197 were shown by mutagenesis to be important for function. These amino acids could not have been predicted based on the available ternary complex crystal structures of the closest AdoMet-dependent homologues, due to sequence divergence and location of the residues in conformationally variable segments. Comparison of the hNNMT, mNNMT, hINMT, and hPNMT crystal structures highlights a surface loop (F27-H31 in hNNMT) that adopts very different conformations in the presence and absence of acceptor substrate and among the different enzymes. The location of this loop near the active site suggests that this region may play a role in substrate access and/or selectivity and might be usefully exploited in future drug design efforts.

■ ASSOCIATED CONTENT

Accession Codes

Coordinates and structure factors have been deposited in the Protein Data Bank with accession code 3ROD.

■ AUTHOR INFORMATION

Corresponding Author

*Phone: (216) 368-1184. Fax: (216) 368-3419. E-mail: vivien. yee@case.edu.

■ ABBREVIATIONS

NNMT, nicotinamide *N*-methyltransferase; wt-hNNMT, wild-type human NNMT; tm-hNNMT, hNNMT K100A/E101A/E103A triple mutant; AdoMet, *S*-adenosyl-L-methionine; AdoHcy, *S*-adenosyl-L-homocysteine; NCA, nicotinamide; MTase, AdoMet-dependent methyltransferase; INMT, indole-thylamine *N*-methyltransferase; PNMT, phenylethanolamine *N*-methyltransferase; DXMT, 3,7-dimethylxanthine methyltransferase.

■ REFERENCES

(1) Aksoy, S., Szumlanski, C. L., and Weinshilboum, R. M. (1994) Human liver nicotinamide N-methyltransferase. cDNA cloning, expression, and biochemical characterization. *J. Biol. Chem. 269*, 14835−14840.

(2) Cantoni, G. L. (1951) Methylation of nicotinamide with soluble enzyme system from rat liver. *J. Biol. Chem. 189*, 203−216.

(3) Williams, A. C., Cartwright, L. S., and Ramsden, D. B. (2005) Parkinson's disease: the first common neurological disease due to auto-intoxication? *QJM 98*, 215−226.

(4) Williams, A. C., and Ramsden, D. B. (2005) Autotoxicity, methylation and a road to the prevention of Parkinson's disease. *J. Clin. Neurosci. 12*, 6−11.

(5) Sartini, D., Muzzonigro, G., Milanese, G., Pierella, F., Rossi, V., and Emanuelli, M. (2006) Identification of nicotinamide N-methyltransferase as a novel tumor marker for renal clear cell carcinoma. *J. Urol. 176*, 2248−2254.

(6) Xu, J., Moatamed, F., Caldwell, J. S., Walker, J. R., Kraiem, Z., Taki, K., Brent, G. A., and Hershman, J. M. (2003) Enhanced expression of nicotinamide N-methyltransferase in human papillary thyroid carcinoma cells. *J. Clin. Endocrinol. Metab. 88*, 4990−4996.

(7) Roessler, M., Rollinger, W., Palme, S., Hagmann, M. L., Berndt, P., Engel, A. M., Schneidinger, B., Pfeffer, M., Andres, H., Karl, J., Bodenmüller, H., Rüschoff, J., Henkel, T., Rohr, G., Rossol, S., Rösch, W., Langen, H., Zolg, W., and Tacke, M. (2005) Identification of nicotinamide N-methyltransferase as a novel serum tumor marker for colorectal cancer. *Clin. Cancer Res. 11*, 6550−6557.

(8) Sartini, D., Santarelli, A., Rossi, V., Goteri, G., Rubini, C., Ciavarella, D., Lo Muzio, L., and Emanuelli, M. (2007) Nicotinamide N-methyltransferase upregulation inversely correlates with lymph node metastasis in oral squamous cell carcinoma. *Mol. Med. 13*, 415−421.

(9) Tomida, M., Mikami, I., Takeuchi, S., Nishimura, H., and Akiyama, H. (2009) Serum levels of nicotinamide N-methyltransferase in patients with lung cancer. *J. Cancer Res. Clin. Oncol. 135*, 1223−1229.

(10) Otwinowski, Z., and Minor, W. (1997) Processing of X-ray Diffraction Data Collected in Oscillation Mode. *Methods in Enzymology* (Carter, C. W., Jr., and Sweet, R. M., Eds.) Vol. 276, pp 307−326, Academic Press, New York.

(11) Vagin, A., and Teplyakov, A. (1997) MOLREP: an automated program for molecular replacement. *J. Appl. Crystallogr. 30*, 1022−1025.

(12) Emsley, P., and Cowtan, K. (2004) Coot: model-building tools for molecular graphics. *Acta Crystallogr. D60*, 2126−2132.

(13) Brunger, A. T., Adams, P. D., Clore, G. M., DeLano, W. L., Gros, P., Grosse-Kunstleve, R. W., Jiang, J. S., Kuszewski, J., Nilges, M., Pannu, N. S., Read, R. J., Rice, L. M., Simonson, T., and Warren, G. L. (1998) Crystallography & NMR system: A new software suite for macromolecular structure determination. *Acta Crystallogr., Sect. D: Biol. Crystallogr. 54*, 905−921.

(14) Murshudov, G. N., Vagin, A. A., and Dodson, E. J. (1997) Refinement of macromolecular structures by the maximum-likelihood method. *Acta Crystallogr. D53*, 240−255.

(15) Laskowski, R. A., MacArthur, M. W., Moss, D. S., and Thornton, J. M. (1993) PROCHECK: a program to check the stereochemical quality of protein structures. *J. Appl. Crystallogr. 26*, 283−291.

(16) DeLano, W. L. (2004) *The PyMOL Molecular Graphics System*, DeLano Scientific LLC, San Carlos, CA (www.pymol.org).

(17) Balducci, E., Emanuelli, M., Raffaelli, N., Ruggieri, S., Amici, A., Magni, G., Orsomando, G., Polzonetti, V., and Natalini, P. (1995) Assay methods for nicotinamide mononucleotide adenylyltransferase of wide applicability. *Anal. Biochem. 228*, 64−68.

(18) van der Spoel, D., Lindahl, E., Hess, B., Groenhof, G., Mark, A. E., and Berendsen, J. J. C. (2005) GROMACS: Fast, flexible, and free. *J. Comput. Chem. 26*, 1701−1718.

(19) van Gunsteren, W. F., Billeter, S. R., Eising, A. A., Hunenberger, P. H., Kruger, P., Mark, A. E., Scott, W. R. P., and Tironi, I. G. (1996) *Biomolecular Simulation: the GROMOS96 Manual and User Guide*, Hochschulverlag AG an der ETZ Zurich, Zurich.

(20) Berendsen, H. J. C., Postma, J. P. M., van Gunsteren, W. F., and Hermans, J. (1981) Interaction models for water in relation to protein hydration, in *Intermolecular Forces* (Pullman, B., Ed.), pp 331−342, D. Reidel Publishing Co., Dordrecht.

(21) Martin, J. L., and McMillan, F. M. (2002) SAM (dependent) I AM: the S-adenosylmethionine-dependent methyltransferase fold. *Curr. Opin. Struct. Biol. 12*, 783−793.

(22) Schubert, H. L., Blumenthal, R. M., and Cheng, X. (2003) Many paths to methyltransfer: a chronicle of convergence. *Trends Biochem. Sci. 28*, 329−335.

(23) Kozbial, P. Z., and Mushegian, A. R. (2005) Natural history of S-adenosylmethionine-binding proteins. *BMC Struct. Biol. 5*, 19.

(24) Holm, L., and Sander, C. (1993) Protein structure comparison by alignment of distance matrices. *J. Mol. Biol. 233*, 123−138.

(25) Drinkwater, N., Gee, C. L., Puri, M., Criscione, K. R., McLeish, M. J., Grunewald, G. L., and Martin, J. L. (2009) Molecular recognition of physiological substrate noradrenaline by the adrenaline-synthesizing enzyme PNMT and factors influencing its methyltransferase activity. *Biochem. J. 422*, 463−471.

(26) McCarthy, A. A., and McCarthy, J. G. (2007) The structure of two N-methyltransferases from the caffeine biosynthetic pathway. *Plant Physiol. 144*, 879−889.

(27) Gee, C. L., Tyndall, J. D. A., Grunewald, G. L., Wu, Q., McLeish, M. J., and Martin, J. L. (2005) Mode of binding of methyl acceptor substrates to the adrenaline-synthesizing enzyme phenylethanolamine N-methyltransferase: implications for catalysis. *Biochemistry 44*, 16875−16885.